Oscillatory Rarefied Gas Flows in Long Capillaries

Alexandros Tsimpoukis, Nikos Vasileiadis, Giorgos Tatsios, and Dimitris Valougeorgis

Abstract Oscillatory, rarefied, linear and nonlinear fully developed flows of single gases and binary gas mixtures, driven by external harmonic mechanisms with arbitrary frequency, have been recently considered by the authors in a series of works. Here, these works are reviewed by focusing on the most notable findings. More specifically, the effects of the oscillation frequency on the velocity overshooting and gas separation phenomena in gas mixture flows and of the oscillation amplitude on the flow pattern in nonlinear single gas flows are presented. Modeling is based in the former case on the McCormack kinetic model and in the latter one on the DSMC method. In general, as the flow becomes more rarefied higher frequencies are needed to trigger the overshooting phenomenon, which becomes more pronounced as the molecular mass of the gas species is increased. Notably, gas separation may be present in the whole range of gas rarefaction, provided that the flow is subject to adequate high oscillation frequency. Finally, the presence of strong external harmonic forces does not significantly affect the oscillatory macroscopic quantities, including the mass flow rate (no distortion of the amplitude-frequency curve), except of the oscillatory axial heat flux, which exhibits a non-sinusoidal pattern.

1 Introduction

Rarefied boundary-driven oscillatory flows of single gases have been extensively investigated over the last two decades [1–7]. These flows are present in various resonator structures [8, 9], while acoustic enhancement or attenuation (even cloaking) may be achieved in viscous-thermal fluids [10]. Propagation of sound waves due to mechanical and thermal excitation through binary gas mixtures has been also considered [11–13].

A. Tsimpoukis (✉) · N. Vasileiadis · G. Tatsios · D. Valougeorgis
University of Thessaly, Volos, Greece
e-mail: atsimpoukis@mie.uth.gr; nikovasi@mie.uth.gr; tatsios@mie.uth.gr; diva@mie.uth.gr

P. Barbante et al. (eds.), *From Kinetic Theory to Turbulence Modeling*, Springer INdAM Series 51, https://doi.org/10.1007/978-981-19-6462-6_20

The corresponding rarefied pressure-driven oscillatory gas flows have attracted much less attention, although there are employed in vapor deposition [14], microfluidic oscillators and pumps [15] and cryogenic pulse tubes [16]. Of course, in the hydrodynamic regime, pressure-driven oscillatory gas flows have been thoroughly examined and are encountered in numerous technological fields ranging from pneumatic lines and control systems [17], reciprocating pumps [18], combustion engines, and bioengineering to enhancement of thermal diffusion in mass and heat transfer processes, species contaminants dispersion and gas separation or mixing [19, 20]. Experimentally, oscillatory-type pressure-driven gas flows may be realized by reciprocating pistons [21] or membranes [22] or by oscillating the channel itself [23].

Although boundary and pressure gradient oscillatory flows have certain similarities, such as the traveling wave disturbance causing the flow, they also have various differences related to the involved physical phenomena and quantities of practical interest. The general mechanisms occurring in oscillatory boundary-driven flows include inertia and viscous forces, while in pressure gradient flows, in addition to the above, pressure forces are also considered. In the latter case, the difference in time scales of pressure and viscous forces may lead to unexpected results, such as the annular effect (velocity overshooting) and enhanced gas separation, which are not observed in former case. Also, in boundary-driven flows we are mainly interested in velocity and shear stresses, while in oscillatory pressure gradient flows including pulsatile flows, we are also interested in the computed flow rates.

Taking into consideration that oscillatory pressure- driven gas flows in the hydrodynamic regime are very common, along with the progress in fabrication techniques of micro devices, it is reasonable to expect that oscillatory pressure-driven rarefied flows of single gases and gas mixtures will be also widely employed, in the short future. Therefore, very recently, some theoretical studies in fully developed oscillatory gas flows in capillaries [24–27] have been reported. Here, the most notable results of the detailed analysis in [24–27] for linear and nonlinear fully developed flows of single gases and binary gas mixtures are presented.

2 Linear Oscillatory Fully Developed Binary Gas Mixture Flow

Consider the time-dependent, isothermal, rarefied flow of a binary gas mixture between two infinite long parallel plates fixed at $y' = \pm H/2$, connecting two containers, as shown in Fig. 1. The pressure in the two containers harmonically oscillates as $\tilde{P}_j\left(t'\right) = \mathbb{R}\left[P_j \exp\left(-i\omega t'\right)\right]$, $j = 1, 2$, resulting in the externally

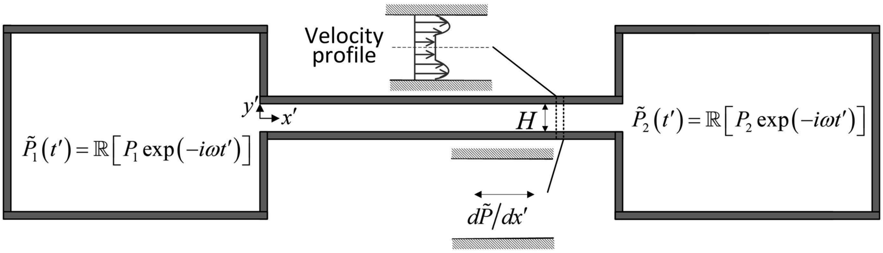

Fig. 1 Oscillatory flow configuration

imposed harmonically oscillating pressure gradient, along the parallel plates, of the form

$$\frac{d\tilde{P}}{dx'} = \mathbb{R}\left[\frac{dP}{dx'} \exp\left(-i\omega t'\right)\right]. \tag{1}$$

Here, $\tilde{P}\left(x', t'\right) = P\left(x'\right)\exp\left(-i\omega t'\right)$ is the oscillatory pressure in the $x'-$ direction parallel to the plates, dP/dx' and ω refer to the amplitude and frequency, respectively, of the oscillatory pressure gradient $d\tilde{P}/dx'$ and t' is the time, while $\mathbb{R}$ denotes the real part of a complex expression $i = \sqrt{-1}$). The well-established assumption that the fluid oscillates in bulk or en mass, i.e., that all quantities oscillate with the same frequency as the pressure gradient, is applied [28]. Thus, this is an harmonically oscillating, fully developed flow (pressure and density remain constant at each cross section, while all other macroscopic distributions depend only in the $y'-$direction normal to the plates).

The binary gas mixture consists of two monatomic species of molecular masses m_α, with the index "$\alpha = 1, 2$," always referring, without loss of generality, to the light and heavy species of the mixture, respectively. The corresponding local number densities of the mixture components, defined by $\tilde{n}_\alpha\left(t'\right)$, oscillate harmonically as $\tilde{n}_\alpha\left(t'\right) = \mathbb{R}\left[n_\alpha \exp\left(-i\omega t'\right)\right]$, where n_α, $\alpha = 1, 2$, is the local amplitude of the oscillating number density of each species. The number density of the mixture is $\tilde{n}\left(t'\right) = \tilde{n}_1\left(t'\right) + \tilde{n}_2\left(t'\right)$, while the molar fraction of the mixture is defined as the ratio of the number density of the light species over the mixture number density, given by $\tilde{C}\left(t'\right) = \mathbb{R}\left[C\exp\left(-i\omega t'\right)\right]$, with $C = n_1/n = n_1/\left(n_1 + n_2\right)$, being the local amplitude of the molar fraction. The molar fraction amplitude of the heavy species is $1 - C$. The mean molecular mass of the mixture is given by $m = Cm_1 + (1 - C)\,m_2$. The number densities of the species and the mixture are related to the corresponding pressures with the equation of states as $\tilde{P}_\alpha = \tilde{n}_\alpha kT$ and $\tilde{P} = \tilde{n}kT$, respectively, where $\tilde{P}_\alpha$ are the partial pressures, $\tilde{P} = \tilde{P}_1 + \tilde{P}_2$ is the total pressure, T is the reference temperature. The mass densities of the species and the mixture are defined as $\rho_\alpha = m_\alpha n_\alpha$ and $\rho = mn$, respectively.

The deduced time-dependent flow quantities of practical interest include the bulk velocity $\tilde{U}_\alpha\left(t', y'\right)$, shear stress $\tilde{\Pi}_\alpha\left(t', y'\right)$ and heat flow $\tilde{Q}_\alpha\left(t', y'\right)$ of the two species $\alpha = 1, 2$, which depend on y', the space independent variable vertical to the plates and vary harmonically with time t' as

$$\tilde{Z}_\alpha\left(t', y'\right) = \mathbb{R}\left[Z_\alpha\left(y'\right)\exp\left(-i\omega t'\right)\right], \tag{2}$$

where $\tilde{Z}_\alpha\left(t', y'\right) = \left[\tilde{U}_\alpha\left(t', y'\right), \tilde{\Pi}_\alpha\left(t', y'\right), \tilde{Q}_\alpha\left(t', y'\right)\right]$, while $\tilde{Z}_\alpha\left(y'\right) = \left[U_\alpha\left(y'\right), \Pi_\alpha\left(y'\right), Q_\alpha\left(y'\right)\right]$ is a vector of the corresponding complex functions. In addition, the oscillatory particle flow rates of the two species are given by $\tilde{J}_\alpha\left(t'\right) = \mathbb{R}\left[J_\alpha \exp\left(-i\omega t'\right)\right]$, where $J_\alpha = n_\alpha \int\limits_{-H/2}^{H/2} U_\alpha dy'$, as well as the corresponding mixture particle flow rate $\tilde{J} = \tilde{J}_1 + \tilde{J}_2$, are complex functions.

Furthermore, the dimensionless independent space and time variables $x = x'/H$, $y = y'/H$and $t = t'\omega$, are introduced. The dimensionless amplitude of the local oscillatory pressure gradient is

$$X = \frac{H}{P\left(x'\right)}\frac{dP\left(x'\right)}{dx'} = \frac{1}{P\left(x\right)}\frac{dP\left(x\right)}{dx} \ll 1. \tag{3}$$

The bulk velocity, shear stress and heat flow in Eq. (2) are nondimensionalized by (υX), $(2PX)$ and (υPX), respectively, with $\upsilon = \sqrt{2kT/m}$ being the characteristic speed of the mixture, to yield:

$$\tilde{\varphi}_\alpha\left(t, y\right) = \mathbb{R}\left[\varphi_\alpha\left(y\right)\exp\left(-it\right)\right] = \varphi_\alpha^{(A)}\left(y\right)\cos\left[t - \varphi_a^{(P)}\left(y\right)\right], \tag{4}$$

where $\tilde{\varphi}_\alpha\left(t, y\right) = \left[\tilde{u}_\alpha\left(t, y\right), \tilde{\varpi}_\alpha\left(t, y\right), \tilde{q}_\alpha\left(t, y\right)\right]$. In Eq. (4) the superscripts (A) and (P) refer to the amplitude and the phase angle, respectively, of each complex quantity.

Furthermore, the flow rates $\tilde{J}_\alpha\left(t'\right)$ are nondimensionalized by $(PXH/m\upsilon)$ to obtain the dimensionless oscillatory particle flow rates of each species

$$\tilde{G}_\alpha\left(t\right) = \mathbb{R}\left[G_\alpha \exp\left(-it\right)\right] = \mathbb{R}\left[G_\alpha^{(A)}\exp\left[i\left(G_\alpha^{(P)} - t\right)\right]\right] = G_\alpha^{(A)}\cos\left[t - G_\alpha^{(P)}\right], \tag{5}$$

where

$$G_\alpha = G_\alpha^{(A)}\exp\left(iG_\alpha^{(P)}\right) = 2\int_{-1/2}^{1/2} u_\alpha dy. \tag{6}$$

Also, the dimensionless oscillatory particle flow rate of the mixture is given by

$$\tilde{G}\,(t) = \mathbb{R}\left[G \exp\left(-it\right)\right] = \mathbb{R}\left[G^{(A)} \exp\left[i\left(G^{(P)} - t\right)\right]\right] = G^{(A)} \cos\left[t - G^{(P)}\right], \tag{7}$$

where $G = CG_1 + (1 - C)\,G_2$, with the superscripts (A) and (P), always referring to amplitudes and phase angles, respectively.

The oscillatory binary gas mixture flow between parallel plates is also characterized by the gas rarefaction and oscillation parameters, given by

$$\delta = \frac{PH}{\mu\upsilon} \quad \text{and} \quad \theta = \frac{P}{\mu\omega}, \tag{8}$$

respectively, where μ is the gas viscosity at some reference temperature T, υ is the characteristic speed of the mixture, the ratio (P/μ) is the intermolecular collision frequency. The composition of the binary gas mixture, i.e., the molecular masses m_1 and m_2, as well as the amplitude of the molar fraction C, must be also specified.

Next, the kinetic formulation, based on the McCormack model [29], is shortly presented. Due to the condition $X \ll 1$ the unknown time-dependent distribution function of each species can be linearized in a standard manner and the linearized distributions are accordingly projected to yield the following set of kinetic equations:

$$\begin{aligned}
&-i\frac{\delta}{\theta}\sqrt{\frac{m_\alpha}{m}}\varPhi_\alpha + c_{\alpha y}\frac{\partial \varPhi_\alpha}{\partial y} + \omega_a \boldsymbol{\gamma}_\alpha \varPhi_a = \\
&-\frac{1}{2}\sqrt{\frac{m}{m_a}} + \omega_\alpha\left\{\boldsymbol{\gamma}_\alpha u_a - \upsilon_{\alpha\beta}^{(1)}\left(u_a - u_\beta\right) - \frac{1}{2}\upsilon_{\alpha\beta}^{(2)}\left(q_a - \frac{m_a}{m_\beta}q_\beta\right) + \right.\\
&+2\sqrt{\frac{m}{m_a}}\left[\left(\boldsymbol{\gamma}_\alpha - \upsilon_{\alpha\alpha}^{(3)} + \upsilon_{\alpha\alpha}^{(4)} - \upsilon_{\alpha\beta}^{(3)}\right)\varpi_a + \upsilon_{\alpha\alpha}^{(4)}\varpi_\beta\right]c_{ay} + \\
&\left.+\frac{2}{5}\left[\left(\boldsymbol{\gamma}_\alpha - \upsilon_{\alpha\alpha}^{(5)} + \upsilon_{\alpha\alpha}^{(6)} - \upsilon_{\alpha\beta}^{(5)}\right)q_a + \upsilon_{\alpha\beta}^{(6)}\sqrt{\frac{m_\beta}{m_a}}q_\beta - \frac{5}{4}\upsilon_{\alpha\beta}^{(2)}\left(u_a - u_\beta\right)\right]\left(c_{ay}^2 - \frac{1}{2}\right)\right\},
\end{aligned} \tag{9}$$

$$\begin{aligned}
&-i\sqrt{\frac{m_\alpha}{m}}\frac{\delta}{\theta}\varPsi_\alpha + c_{\alpha y}\frac{\partial \varPsi_\alpha}{\partial y} + \omega_\alpha \boldsymbol{\gamma}_\alpha \varPsi_a = \\
&= \frac{4}{5}\omega_\alpha\left[\left(\boldsymbol{\gamma}_\alpha - \upsilon_{\alpha\alpha}^{(5)} + \upsilon_{\alpha\alpha}^{(6)} - \upsilon_{\alpha\beta}^{(5)}\right)q_a + \upsilon_{\alpha\beta}^{(6)}\sqrt{\frac{m_\beta}{m_a}}q_\beta - \frac{5}{4}\upsilon_{\alpha\beta}^{(2)}\left(u_a - u_\beta\right)\right].
\end{aligned} \tag{10}$$

Here, $\varPhi_a$ and $\varPsi_a$ are complex perturbed distribution functions for each species, $\omega_\alpha = \delta\left(C/\gamma_1 + (1 - C)/\gamma_2\right)\sqrt{m_a/m}$ and $\gamma_a \quad (a = 1, 2)$ are the collision frequencies of each species [30]. Also, $\alpha, \beta = 1, 2$, with $\alpha \neq \beta$, while the expressions for the quantities $\nu_{\alpha\beta}^{(k)}$ are given in terms of the Chapman-Cowling integrals as in [30]. The macroscopic quantities u_α, ϖ_α and q_α at the right hand side of Eqs. (9) and (10) are defined in Eq. (4), respectively, and after applying the linearization and projection procedures, they are obtained as moments of Φ_α and Ψ_α as follows:

$$u_\alpha(y) = \frac{1}{\sqrt{\pi}} \int_{-\infty}^{\infty} \Phi_a \exp\left(-c_{ay}^2\right) dc_{ay}, \tag{11}$$

$$\varpi_\alpha(y) = \frac{1}{\sqrt{\pi}} \sqrt{\frac{m_a}{m}} \int_{-\infty}^{\infty} \Phi_a c_{ay} \exp\left(-c_{ay}^2\right) dc_{ay}, \tag{12}$$

$$q_\alpha(y) = \frac{1}{\sqrt{\pi}} \int_{-\infty}^{\infty} \left[\Psi_a + \left(c_{ay}^2 - \frac{1}{2}\right) \Phi_a\right] \exp\left(-c_{ay}^2\right) dc_{ay}. \tag{13}$$

In the present work purely diffuse reflection at the walls is assumed.

The above set of equations is computationally solved based on the discrete velocity method in the c_y space and on the second-order diamond finite difference scheme in the y space. The discretized equations are solved in an iterative manner between the kinetic equations (9) and (10) and the moment equations (11)–(13). More information about the numerical scheme may be found in [27].

Computational results are presented for the mixture flow rate amplitude and phase angle (Fig. 2), the velocity and shear stress distributions (Fig. 3) and the ratio of the flow rate amplitudes of the species (Fig. 4) in a wide range of the gas rarefaction and oscillation parameters δ and θ, as well as of the molar fraction $C \in [0, 1]$ for the He–Xe mixture with $m_2/m_1 = 32.8$.

In Fig. 2, the He–Xe flow rate amplitude $G^{(A)}$ and phase angle $G^{(P)}$ are presented in terms of δ, with $\theta = [1, 100]$ and $C = [0, 0.5, 0.9]$. The results with $C =$

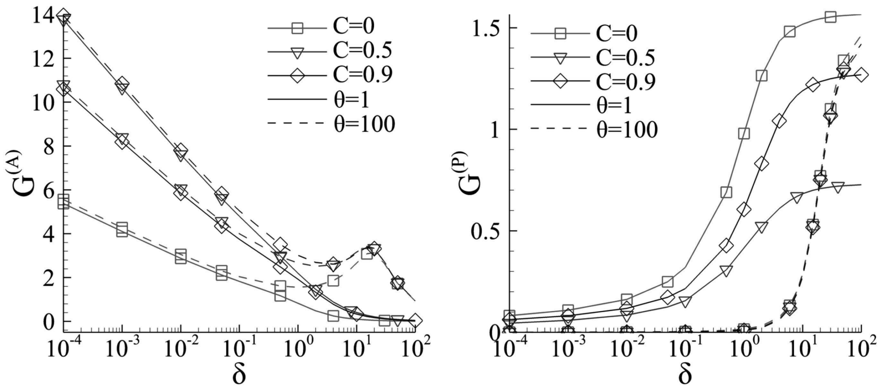

Fig. 2 Mixture flow rate amplitude $G^{(A)}$ and phase angle $G^{(P)}$ of He-Xe vs δ

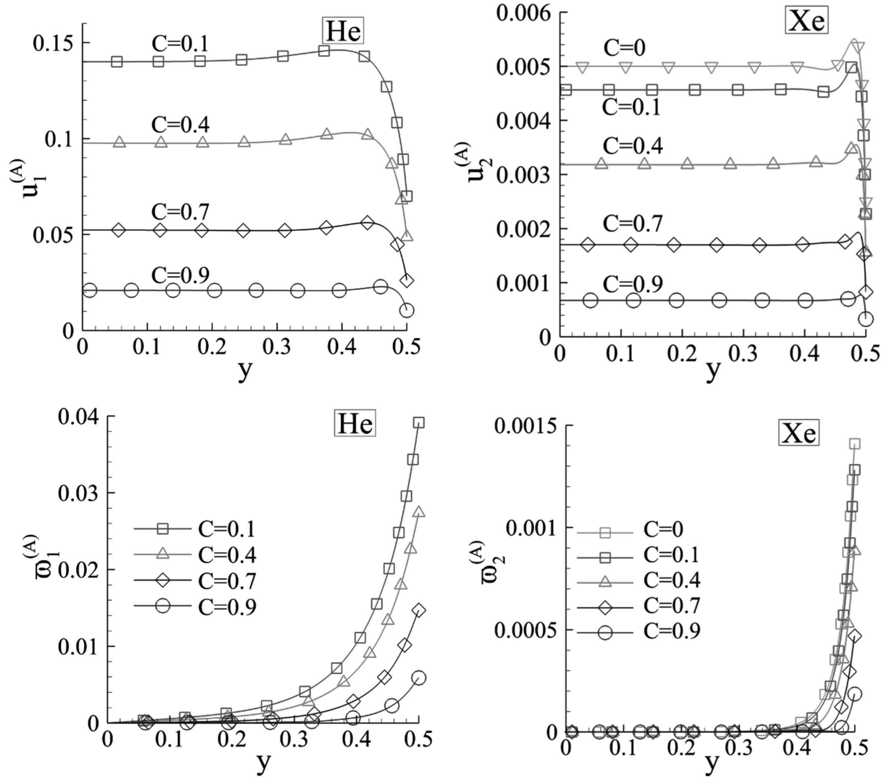

Fig. 3 Velocity $u_\alpha^{(A)}(y)$ and shear stress $\varpi_\alpha^{(A)}(y)$ amplitudes of each species of He-Xe for $\delta = 10$ and $\theta = 0.1$. Reprinted with permission from [27]. Copyright (2022) by the American Physical Society

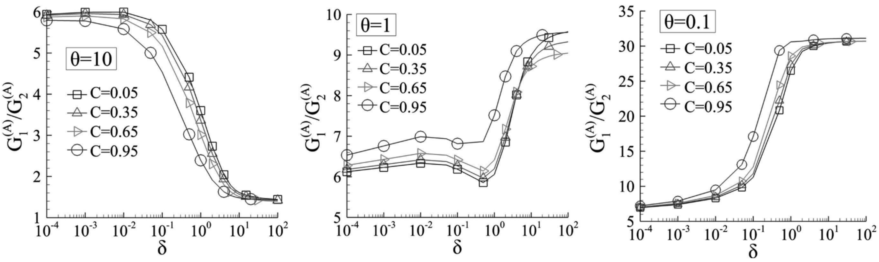

Fig. 4 Ratio of flow rate amplitudes $G_1^{(A)}/G_2^{(A)}$ of the species of He-Xe vs $\delta \in [10^{-4}, 10^2]$. Reprinted with permission from [27]. Copyright (2022) by the American Physical Society

0 correspond to the oscillatory single gas flow reported in [25]. The flow rate amplitudes and phase angles of the mixture ($C \neq 0$) depend on the flow parameters similarly to the corresponding single gas ones ($C = 0$). Always, the mixture flow

rate amplitude is larger and the phase angle is smaller than the corresponding ones of the single gas. At large θ the dependency of $G^{(A)}$ on δ, is not monotonic, indicating that there is a critical δ to obtain the maximum flow rate, while at small θ, $G^{(A)}$ is decreased monotonically. This is due to the fact that at low oscillation frequencies and as long as $\delta \ll \theta$, the variation of $G^{(A)}$ with δ has some resemblance with the steady one, including the presence of the Knudsen minimum. Then, as δ is further increased the effect of the inertia forces becomes significant and $G^{(A)}$ is decreased. In addition, as θ is decreased (the oscillation frequency is increased), $G^{(A)}$ is always decreased, while $G^{(P)}$ (the phase angle lag with respect to the pressure gradient) is always increased reaching the limiting value of $\pi/2$.

In Fig. 3, the distributions of the velocity and shear stress amplitudes $u_\alpha^{(A)}(y)$ and $\varpi_\alpha^{(A)}(y)$ of each species of the He–Xe gas mixture, with $C = [0.1, 0.4, 0.7, 0.9]$, are provided for $\delta = 10$ and $\theta = 0.1$. The specific values of δ and θ are suitable for investigating the velocity overshooting phenomenon in the light and heavy species of the mixture. Velocity overshooting is due to the fact that close to the wall, viscous and pressure gradient forces actually add to each other due to the large phase angle lag between them. As a result, the combined effect accelerates the fluid to higher velocities than those produced in the core by the pressure gradient forces acting alone. For Xe, compared to He, the velocity overshooting becomes sharper, appearing, along with its maximum value, closer to the wall inside a much thinner layer. In the core of the flow, the velocity amplitudes of both He and Xe become flat and they are close to the corresponding analytical amplitudes $u_\alpha^{(A)} = (\theta/2\delta)(m/m_\alpha)$ (see Section 3 in [27]). In parallel, $\varpi_\alpha^{(A)}(y)$ for both He and Xe take their highest values at the wall and they are monotonically decreased towards the channel center. The attenuation of the shear stress amplitude of He is smooth, diffused in the whole distance from the wall to the center, while the one of Xe is rapid in a narrow zone close to the wall and far from the wall the shear stress of Xe becomes zero. Since the viscous forces in the case of He act in the whole distance between the plates, while in the case of Xe only in thin zones close to the walls, the above observations on the velocity overshooting of He and Xe are physically justified. This description of the velocity and shear stress amplitudes remains valid for all molar fractions tested [27]. In brief, it is seen that as the molecular mass of the gas species increases, the species shear stress, which is created at the wall and is diffused into the flow, attenuates more rapidly, i.e., the Stokes layer becomes thinner and the Richardson effect more pronounced. Velocity overshooting may be also present in even lower rarefaction parameters provided that higher oscillation frequencies are applied [24].

The gas separation phenomenon for various values of δ and θ is discussed next. Gas separation in rarefied steady-state pressure-driven binary gas flows though capillaries may be analyzed by computing the ratio of the particle flow rates J_1/J_2, which is monotonically increased as δ is decreased up to its maximum value, equal to $\sqrt{m_2/m_1}(1-C)/C$, in the free molecular limit ($\delta \to 0$) [31].

In Fig. 4, the ratio of the flow rate amplitudes $G_1^{(A)}/G_2^{(A)}$ is provided in terms of δ for the He–Xe gas mixture, with $C = [0, 05, 0.35, 0.65, 0.95]$ and $\theta = [0.1, 1, 10]$.

At $\theta = 10$ the ratio $G_1^{(A)}/G_2^{(A)}$ varies qualitatively similarly as in the steady-state binary gas flow setup. It is about constant or slightly reduced in the free molecular regime (at $\delta = 0$ it is equal to the corresponding steady one) and then it is monotonically decreased asymptotically going in the slip and hydrodynamic regimes to one. In the free molecular regime, with regard to the gas rarefaction parameter, as $\delta \to 0$, with $\theta > 0$, Eqs. (9) and (10) tend to the corresponding ones for steady-state binary gas flow in the free molecular limit [30]. However, at $\theta = 1$ and $\theta = 0.1$ the behavior of $G_1^{(A)}/G_2^{(A)}$ is completely different. It remains about constant in free molecular regime, but then, it is increased in the transition regime and finally, as δ further increases, it keeps asymptotically increasing to some constant value, which is the molecular mass ratio of the heavy over the light species m_2/m_1 ($G_{He}^{(A)}/G_{Xe}^{(A)} = 32.8$). This is in accordance to the closed-from expression that as $\theta \to 0$, $G_1/G_2 = m_2/m_1$ [27]. This behavior, with the minimum and maximum values of $G_1^{(A)}/G_2^{(A)}$ appearing at the free molecular and hydrodynamic limits, respectively, and the increase in the transition regime (completely reversed compared to the steady-state behavior) becomes more pronounced as θ is decreased.

It is evident that the oscillation parameter θ has a dominant effect on the amplitude ratio of He over Xe, which is significantly increased as θ is decreased (at $\theta = 0.1$ the flow rate amplitude of He is about thirty times larger than of Xe). This behavior is due to the corresponding behavior of the velocity amplitudes and it is contributed to inertia forces, which are increased with the oscillation frequency and they influence the bulk velocity amplitude of the heavy species much more than of the light one. Therefore, as θ is decreased, the flow rate amplitude of the heavy species decreases much more significantly than the light one and although both amplitudes are decreased the velocity amplitude ratio of the light over the heavy species is increased. This effect is magnified as the flow becomes less rarefied overcoming diffusion effects due to increased intermolecular collisions and therefore, as δ increases the amplitude ratio keeps increasing. There is no contradiction to general theory, since oscillatory flows approach the hydrodynamic regime, only when both δ and θ are adequately large.

3 Nonlinear Oscillatory Fully Developed Single Gas Flow

Consider the oscillatory nonlinear fully developed flow of a monatomic rarefied gas, confined between two parallel infinite plates at temperature T_0 located at $y' = \pm H/2$, due to an external harmonic force acting on the gas per unit mass in the $x-$direction parallel to the plates [26]. The external force is defined as $\tilde{F}'\left(\omega,\ t'\right) = F' \cos\left(\omega\, t'\right)$, where F' is the force amplitude. The convenient complex factor $\exp\left(-i\omega t'\right)$ previously used, cannot be employed since the force amplitude F' may be arbitrarily large and in nonlinear oscillatory flows the real and imaginary parts are not separable.

The oscillatory macroscopic distributions of practical interest, characterizing the flow, include the x−component $U_{x'}\left(y', t'\right)$ of the velocity vector, the number density $N\left(y', t'\right)$, the temperature $T\left(y', t'\right)$, and the axial and normal heat flow components $Q_{x'}\left(y', t'\right)$ and $Q_{y'}\left(y', t'\right)$, respectively, with $-H/2 \le y' \le H/2$ and $0 \le t' \le 2\pi/\omega$. The most important overall quantities are the mass flow rate and axial heat flow

$$M'\left(t'\right) = m \int_{-H/2}^{H/2} N\left(y', t'\right) U_{x'}\left(y', t'\right) dy' \text{ and } \bar{Q}_{x'}\left(t'\right) = \frac{1}{H} \int_{-H/2}^{H/2} Q_{x'} dy', \tag{14}$$

respectively, where m is the molecular mass.

The parameters defining the above dimensional flow setup include the rarefaction parameter and oscillation parameter defined in Eq. (8). Also, the external force parameter, defined as $F = F'H/\upsilon_0^2$, is needed. It is the inverse of the square of the Froude number (Fr). The effect of the external force on the flow is increased with F and nonlinear effects are becoming dominant. On the contrary, as F is decreased the corresponding linear oscillatory flow, which is linearly proportional to the force magnitude, is gradually recovered.

The following dimensionless variables are introduced:

$$x = \frac{x'}{H}, dx = \frac{dx'}{H}, y = \frac{y'}{H}, dy = \frac{dy'}{H}, t = \frac{t'}{(H/\upsilon_0)} \tag{15}$$

$$n = \frac{N}{N_0}, u_x = \frac{U_{x'}}{\upsilon_0}, \tau = \frac{T}{T_0}, p_{xy} = \frac{\boldsymbol{\Pi}_{x'y'}}{2P_0}, p = \frac{\boldsymbol{P}}{2P_0}, q_x = \frac{Q_{x'}}{\upsilon_0 P_0}, q_y = \frac{Q_{y'}}{\upsilon_0 P_0}. \tag{16}$$

The equation of state becomes $p = n\tau/2$.

Then, the dimensionless external force acting on the gas per unit mass becomes

$$\tilde{F}\left(\delta, \theta,\ t\right) = F \cos\left(\frac{\delta}{\theta}\, t\right), \tag{17}$$

while the dimensionless flow rate and axial heat flow are given by

$$M(t) = \frac{M'}{2P_0\left(H/\upsilon_0\right)} = \int_{-1/2}^{1/2} n(t, y)\, u(t, y)\, dy, \quad \bar{q}_x(t) = \int_{-1/2}^{1/2} q_x(y, t)\, dy. \tag{18}$$

Next, the typical DSMC approach, with the No Time Counter (NTC) scheme proposed by Bird [32], is implemented. The time evolution of the particle system within a small time interval $\Delta t'$ is split into two consecutive steps: free motion of all particles and binary collisions of particles. The time step $\Delta t'$ is nondimensionalized as $\Delta t = \Delta t' / (H/\upsilon_0)$. Purely diffuse boundary conditions are considered at the walls, while periodic boundary conditions are applied in the $x-$ and $z-$ directions. Hard sphere (HS) molecules are assumed. The external force is introduced by accordingly altering the particle velocities at each time step, during the free motion.

Numerical results of the dimensionless flow rate and axial heat flow are provided in terms of the force amplitude $F = [0.05, 0.1, 0.5]$, corresponding to small, moderate, and large force amplitudes, in a wide range of δ and θ. Since the results of the nonlinear gas flow are similar with the linear ones in terms of δ and θ, only the effect of the force amplitude is here discussed.

In Fig. 5, the flow rate amplitudes G_A are divided by the external force F in order to directly compare with the corresponding linear results (the linear solution is proportional to F) and they are presented for $\delta = [0.1, 1, 10]$, $\theta = \left[0.1, 1, 10, 20, 10^2\right]$ and $F = [0.05, 0.1, 0.5]$. The linear flow rate amplitudes obtained in [26] are also provided. It is seen that for $F = 0.05$ and $F = 0.1$ the deviation between the corresponding DSMC and linear solutions is small for $\delta \geq 1$ and for all values of θ, while for $\delta = 0.1$ and $\theta = [10, 20, 10^2]$ the deviation is increased. It is evident that nonlinear effects are becoming more pronounced in highly rarefied atmospheres (small δ) and low frequencies (large θ). For $F = 0.5$ all deviations between DSMC and linear results are further increased due to nonlinear effects. Again, the largest deviations are occurring at $\delta = 0.1$ and $\theta = [10, 20, 10^2]$ ($\delta << \theta$), while the deviations remain small for $\delta \geq 1$, even at high frequencies. Overall, it may be stated that the presence of strong external harmonic forces does not significantly affect the mass flow rate of the oscillatory flow, i.e., there is no distortion of the amplitude-frequency response curve.

The space-average axial flow $\bar{q}_x(t)$ is plotted over one cycle in Fig. 6 for $\delta = [0.1, 1, 10]$ and $\theta = \left[0.1, 1, 10, 20, 10^2\right]$ with $F = [0.05, 0, 5]$. It is readily seen that there are significant qualitative differences between the corresponding space-average heat flow for $F = 0.05$ and $F = 0.5$. For $F = 0.05$, $\bar{q}_x(t)$ for all values of δ and θ has a sinusoidal behavior over time. For $F = 0.5$, $\bar{q}_x(t)$ shows over one cycle various patterns. It is seen that for $\delta = 0.1$ with $\theta = 0.1$, $\delta = 1$ with $\theta = [0.1, 1]$ and for $\delta = 10$ and $\theta = [0.1, 1, 10]$, i.e., in all cases

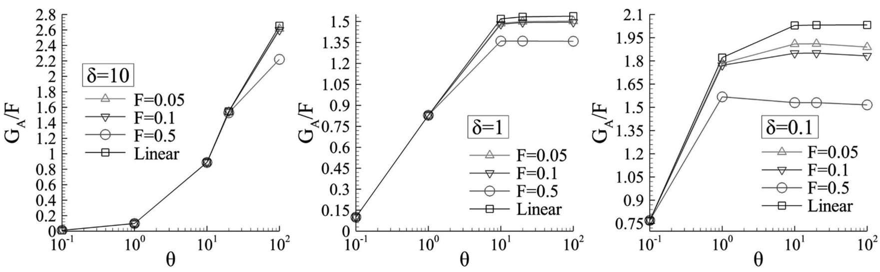

Fig. 5 Normalized oscillatory flow rate amplitude G_A/F vs $\theta \in \left[10^{-1}, 10^2\right]$

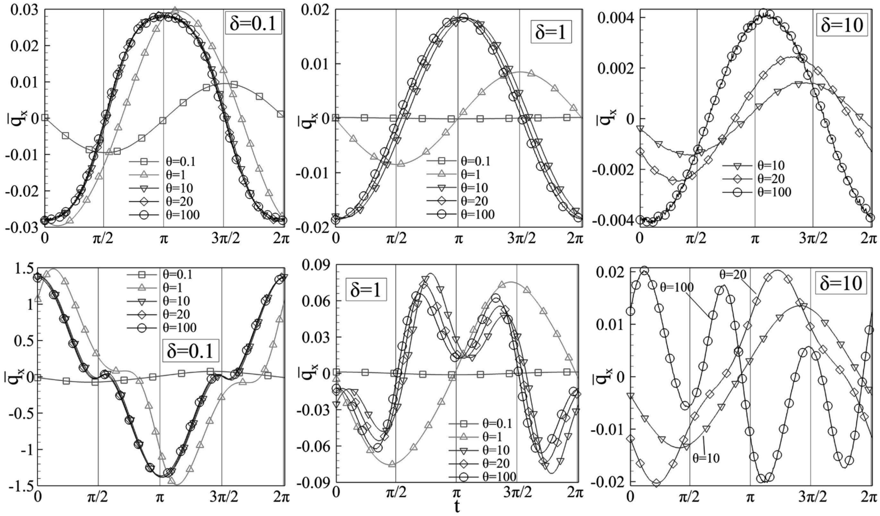

Fig. 6 Space-average axial heat flux $\bar{q}_x\ (t)$ vs t with $F = 0.05$ (up) and $F = 0.5$ (down) and $\theta = [0.1, 1, 10, 20, 100]$. Reproduced from [26], with the permission of AIP Publishing

where $\delta \geq \theta$, $\bar{q}_x\ (t)$ exhibits a sinusoidal pattern. On the contrary, in all cases where $\delta < \theta$, $\bar{q}_x\ (t)$ exhibits a rather complex non-sinusoidal pattern indicating that the introduced nonlinearities are responsible for the generation of oscillatory motion containing several harmonics. These results are in agreement with the discussion in Fig. 5, where nonlinear effects are becoming more significant in highly rarefied flow (small δ) and low oscillation frequencies (large θ). Also, for both values of F, the amplitude of $\bar{q}_x\ (t)$, as of all other macroscopic quantities, is reduced with θ and almost diminishes at very high frequencies, particularly as the gas becomes less rarefied.

4 Concluding Remarks

A brief overview of rarefied, oscillatory, pressure-driven, linear and nonlinear, fully developed flows of single gases and binary gas mixtures is provided, while the detailed analysis may be found in [24–27]. Here, the discussion is focused on the most notable findings, which include velocity overshooting, gas separation and nonlinear effects. The following concluding remarks are stated:

- Velocity overshooting (or the so-called Richardson effect) is present in oscillatory, rarefied single and binary gas mixture flows, but as the flow becomes more rarefied higher frequencies are needed to trigger this phenomenon.

- Gas separation in oscillatory binary gas mixture, may be present in the whole range of gas rarefaction provided that the flow is subject to adequate high oscillation frequency.
- Range of applicability of linear theory is much wider than expected in terms of the imposed amplitude of the oscillatory pressure gradient. The oscillatory axial heat flux is the mostly affected quantity and the only one that, due to nonlinearities, may exhibit a complex pattern.

The present results may be useful in the design of technological devices operating at moderate and high frequencies in the whole range of gas rarefaction, applicable in various technological fields.

Acknowledgments This work has been carried out within the framework of the EUROfusion Consortium and has received funding from the Euratom research and training programme 2014-2018 and 2019-2020 under grant agreement No 633053. The views and opinions expressed herein do not necessarily reflect those of the European Commission. Part of this work has been performed by using computational resources provided by the MARCONI-FUSION HPC.

References

1. Hadjiconstantinou, N.G.: Sound wave propagation in transition-regime micro- and nanochannels. Phys. Fluids **14**, 802–809 (2002)
2. Sharipov, F., Kalempa, D.: Oscillatory Couette flow at arbitrary oscillation frequency over the whole range of the Knudsen number. Microfluid. Nanofluidics **4**, 363–374 (2008)
3. Desvillettes, L., Lorenzani, S.: Sound wave resonances in micro-electro-mechanical systems devices vibrating at high frequencies according to the kinetic theory of gases. Phys. Fluids **24**, 1–24 (2012)
4. Struchtrup, H.: Resonance in rarefied gases. Contin. Mech. Thermodyn. **24**, 361–376 (2012)
5. Taguchi, S., Takata, S.: Vacuum formation behind the expansion wave in a piston motion problem. Phys. Rev. E Stat. Nonlinear Soft Matt. Phys. **86**, 016305 (2012)
6. Aoki, K., Kosuge, S., Fujiwara, T., Goudon, T.: Unsteady motion of a slightly rarefied gas caused by a plate oscillating in its normal direction. Phys. Rev. Fluids **2**, 1–33 (2017)
7. Wang, P., Zhu, L., Su, W., Wu, L., Zhang, Y.: Nonlinear oscillatory rarefied gas flow inside a rectangular cavity. Phys. Rev. E **97**, 43103 (2018)
8. Lorenzani, S., Gibelli, L., Frezzotti, A., Frangi, A., Cercignani, C.: Kinetic approach to gas flows in microchannels. Nanoscale Microscale Thermophys. Eng. **11**, 211–226 (2007)
9. Tsimpoukis, A., Valougeorgis, D.: Linear harmonic oscillatory rarefied gas flow with arbitrary frequency in comb finger blocks. Sensors Actuators A Phys. **331**, 112997 (2021)
10. Ben-Ami, Y., Manela, A.: The sound of a pulsating sphere in a rarefied gas: continuum breakdown at short length and time scales. J. Fluid Mech. **871**, 668–693 (2019)
11. Bisi, M., Lorenzani, S.: High-frequency sound wave propagation in binary gas mixtures flowing through microchannels. Phys. Fluids **28**, 052003 (2016)
12. Kalempa, D., Sharipov, F., Silva, J.C.: Sound waves in gaseous mixtures induced by vibro-thermal excitation at arbitrary rarefaction and sound frequency. Vacuum **159**, 82–98 (2019)
13. Zhang, Y., Wang, P., Guo, Z.: Oscillatory square cavity flows of binary gas mixtures. Phys. Fluids **33**, 067121 (2021)
14. Abreu, R.A., Troup, A.P., Sahm, M.K.: Causes of anomalous solid formation in the exhaust systems of low-pressure chemical vapor deposition and plasma enhanced chemical vapor deposition semiconductor processes. J. Vacuum Sci. Technol. B Microelectron. Nanometer Struct. Process. Measur. Phenomena **12**, 2763–2767 (1994)

15. Wang, S. et al.: On the modelling of the switching mechanisms of a Coanda fluidic oscillator. Sensors Actuators A Phys. **299**, 111618 (2019)
16. Jousten, K.: Applications and scope of vacuum technology. In: Jousten, K (ed.) Handbook of Vacuum Technology, pp. 19–28. Wiley-VCH Verlag GmbH & Co. KGaA, Weinheim (2016)
17. Stecki, J.S., Davis, D.C.: Fluid transmission lines–distributed parameter models part 1: a review of the state of the art. Proc. Inst. Mech. Eng. Part A Power Proc. Eng. **200**(4), 215–228 (1986)
18. Karassik, I.J., Messina, J.P., Cooper, P., Heald, C.C.: Pump Handbook. McGraw-Hill, New York (2000)
19. Kurzweg, U.H.: Enhanced heat conduction in oscillating viscous flows within parallel-plate channels. J. Fluid Mech. **156**, 291 (1985)
20. Brereton, G.J., Jalil, S.M.: Diffusive heat and mass transfer in oscillatory pipe flow. Phys. Fluids **29**, 073601 (2017)
21. Jaeger, M.J., Soepardi, T., Maddahian, A., Kurzweg, U.: Diffusional separation of gases and solutes in oscillatory flow. Sep. Sci. Technol. **26**, 503–514 (1991)
22. Jalil, S.M.: Experimental and numerical investigation of axial heat transfer enhancement by oscillatory flows. Int. J. Therm. Sci. **137**, 352–364 (2019)
23. Thomas, A.M.: Unusual effects of oscillating flows in an annulus on mass transfer and separation. Adv. Sp. Res. **32**, 279–285 (2003)
24. Tsimpoukis, A., Valougeorgis, D.: Rarefied isothermal gas flow in a long circular tube due to oscillating pressure gradient. Microfluid. Nanofluidics **22**, 5 (2018)
25. Tsimpoukis, A., Valougeorgis, D.: Pulsatile pressure driven rarefied gas flow in long rectangular ducts. Phys. Fluids **30**, 047104 (2018)
26. Tsimpoukis, A., Vasileiadis, N., Tatsios, G., Valougeorgis, D.: Nonlinear oscillatory fully-developed rarefied gas flow in plane geometry. Phys. Fluids **31**, 067108 (2019)
27. Tsimpoukis, A., Naris, S., Valougeorgis, D.: Oscillatory pressure-driven rarefied binary gas mixture flow between parallel plates. Phys. Rev. E **103**, 033103 (2021)
28. Zamir, M.: The Physics of Pulsatile Flow. Springer, New York (2000)
29. McCormack, F.J.: Construction of linearized kinetic models for gaseous mixtures and molecular gases. Phys. Fluids **16**, 2095 (1973)
30. Naris, S., Valougeorgis, D., Kalempa, D., Sharipov, F.: Gaseous mixture flow between two parallel plates in the whole range of the gas rarefaction. Phys. A Stat. Mech. its Appl. **336**, 294–318 (2004)
31. Valougeorgis, D., Vargas, M., Naris, S.: Analysis of gas separation, conductance and equivalent single gas approach for binary gas mixture flow expansion through tubes of various lengths into vacuum. Vacuum **128**, 1–8 (2016)
32. Bird, G.A.: Molecular Gas Dynamics and the Direct Simulation of Gas Flows. Clarendon Press, Oxford (1994)